Hindawi
International Journal of RF and Microwave Computer-Aided Engineering
Volume 2023, Article ID 2437462, 7 pages
https://doi.org/10.1155/2023/2437462

Research Article

Design of Filtering Coupler Based on Patch Resonator with High Selectivity

Xu Shi, Qian Zhang, Shuokun Ma, Han Zhang, Xiang Gao, Rui Li, and Gang Zhang

School of Electrical and Automation Engineering, Nanjing Normal University, Nanjing 210046, China

Correspondence should be addressed to Xiang Gao; gaoxiang@njnu.edu.cn

Received 15 November 2022; Revised 29 April 2023; Accepted 27 July 2023; Published 10 August 2023

Academic Editor: Bhaskar Gupta

In this paper, a new approach for designing a planar high frequency selectivity filtering coupler based on a circular patch resonator is proposed. In order to explain the operating principle, the resonant property of the circular patch resonator has been investigated firstly. Two circular patch resonators connected by two microstrip lines are used in this design. A filtering coupler is achieved by adjusting the feeder position and the length and width of the microstrip line used to connect the two resonators. Without additional circuits, the desired 0° and 180° phase differences are realized by the inherent in-phase and out-of-phase characteristics of E-fields at the TM_{11} mode. To improve the passband selectivity, transmission zeros are created by introducing a coupling between the source and load through the coupling slots etched on the ground. Finally, a prototype of the filtering coupler centered at 2.12 GHz is designed, implemented, and tested, while the measured results coincide well with simulated ones, verifying the proposed design concept.

1. Introduction

In recent years, with the rapid development of modern wireless communication systems, integrated functional RF components have become the key devices of various communication standards [1]. As components in wireless communication systems, the filter and coupler play important roles in many RF/microwave applications. In wireless communication systems, filters and couplers are usually cascaded together, which will cause high insertion loss and large size. In order to overcome these problems, the filtering coupler, a functional integrated device with a filtering function and coupler function, has gradually become a research hotspot [2–10].

Most of the filtering couplers can be classified into three main categories according to different resonator formats, transmission line resonators [2–6], substrate-integrated waveguide (SIW) resonators [7, 8], and patch resonators [9–10]. The first kind commonly suffers from high conductor loss. SIW and patch resonators overcome these drawbacks. Compared with SIW, patch resonators are much simpler and more straightforward in analysis and design. As a result, the patch resonator is a good candidate for the design of the filtering coupler. Preliminary progress has been made in the study of filtering couplers based on the patch resonator [9, 10]. In [9], a multilayer coupler has been developed based on a circular patch resonator. However, its geometry is complicated, and the frequency selectivity needs to be improved due to the lack of transmission zeros. In [10], a balanced-to-unbalanced filtering coupler has also been explored by virtue of the patch resonators in the back-to-back form. Although good balanced filtering performance has been achieved, additional etched quarter-wavelength ($\lambda/4$) microstrips open stubs with different lengths to create two transmission zero (TZ) results in a relative large size, and the stacked configuration increases the design complexity.

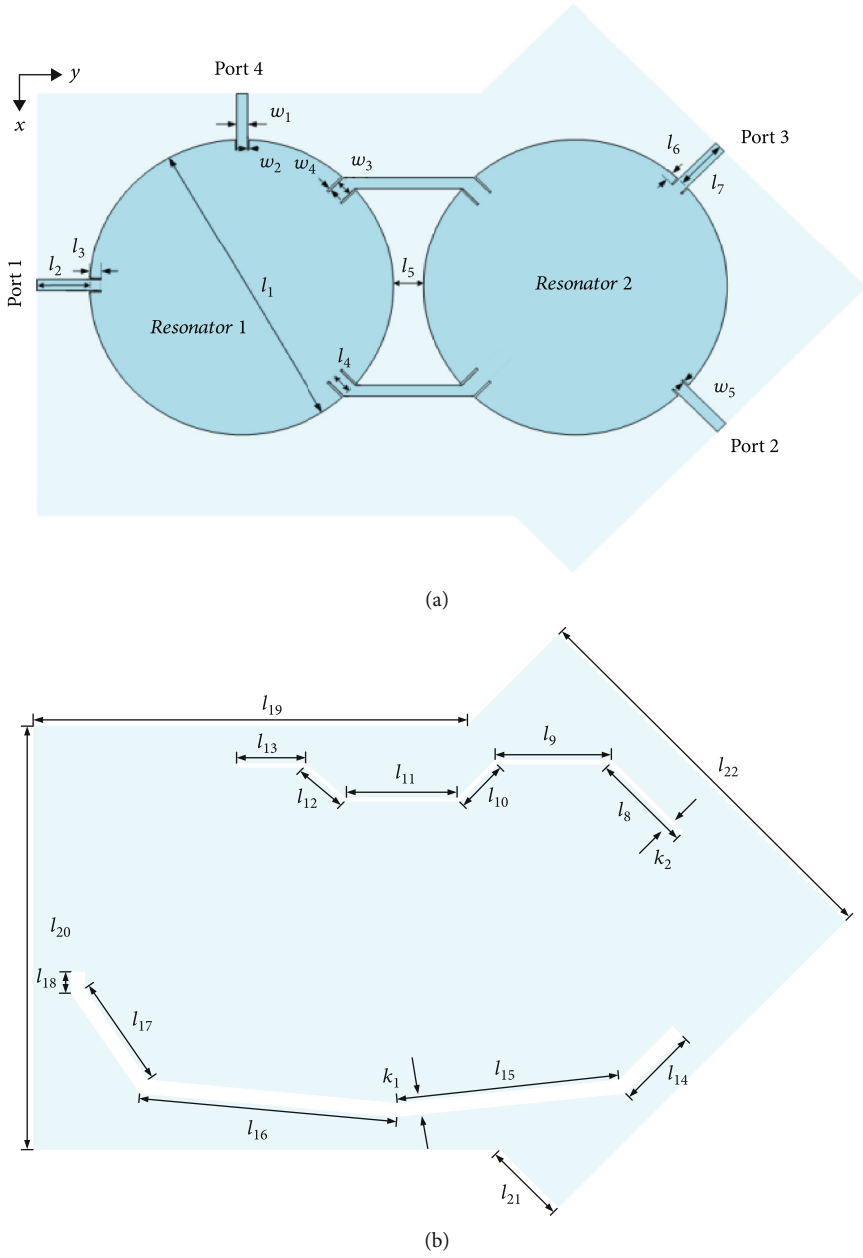

Figure 1: Layout of the proposed filtering coupler: (a) top view; (b) bottom view.

In this paper, a new design of a high frequency selectivity planar filtering coupler by utilizing the circular patch resonators is proposed. Originating from the resonating properties of the circular patch resonator, a prototype of the filtering coupler is proposed by virtue of two elaborately connected circular patch resonators. Afterwards, the desire for 0° and 180° phase differences, good return loss, and isolation between two output ports are realized simultaneously. Furthermore, due to the introduction of a source-load coupling path, two transmission zeros are created, enabling high frequency selectivity.

2. Design and Analysis

Figure 1 shows the layout of this design. It consists of two circular patch resonators and four ports, where port 1 and

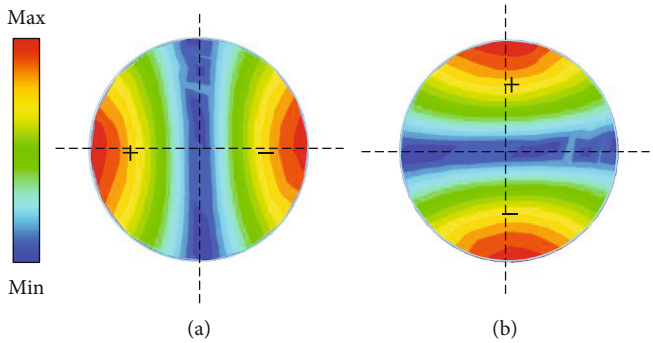

Figure 2: E-field distributions of degenerate mode TM_{11}: (a) TM_{11a} mode; (b) TM_{11b} mode.

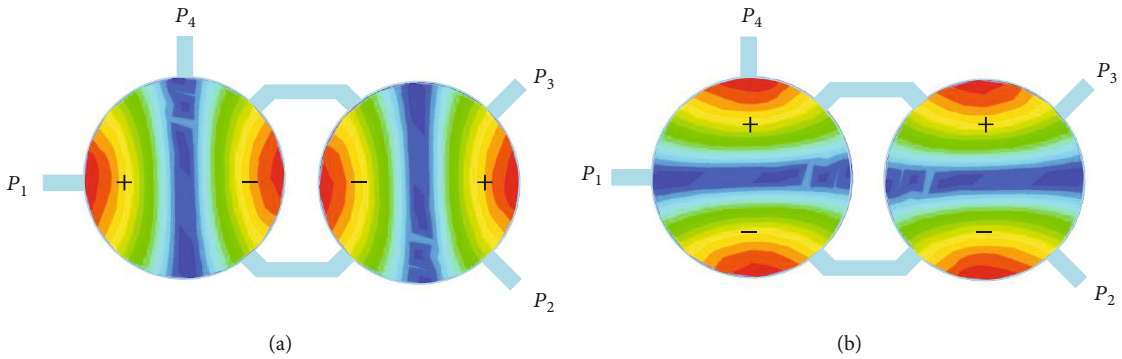

FIGURE 3: E-field distributions under different port excitations: (a) port 1 excitation; (b) port 4 excitation.

port 4 are located at the resonator 1, while port 2 and port 3 are located at the resonator 2. The two patch resonators are connected by two microstrip lines. All lines are optimized by insetting into the circular patch resonator. There are two coupling slots located on the ground, connecting one input port and one output port.

Firstly, the E-field distribution of the TM_{11} mode and resonance properties of the circular patch resonator is fully considered. The patch resonator can be deemed as a waveguide cavity with magnetic walls along the sides, where a similar cavity model theory can be utilized to derive the resonant frequencies of the orthogonal degenerate TM_{11} modes as [5]

$$f_{nm} = \frac{X_{nm}c}{2\pi R_e\sqrt{\varepsilon_r}}, X_{11} = 1.84118, \quad (1)$$

$$R_e = R\left[1 + \frac{2h}{\pi R\varepsilon_r}\left(\ln\frac{\pi R}{2h} + 1.77226\right)\right]^{1/2}, \quad (2)$$

where c is the speed of light in free space while ε_r is the relative permittivity of the substrate and R is the radius of the circular patch resonator. h represents the thickness of the dielectric substrate. The resonant frequencies and E-field distributions can be investigated by executing a full-wave simulation.

Figure 2 shows the E-field distribution of the degenerate TM_{11} modes. These modes are symmetrical along a symmetric line which is orthogonal to the input ports, and the E-field distribution along the symmetric line is zero. Since the two TM_{11} modes are orthogonal to each other, the two input ports are orthogonal to each other. Since the two patch resonators are connected by two microstrip lines, the E-field distribution of the right patch resonator is the same as the left one. Through adjustment of the location of the two output ports, the desire for 0° and 180° phase differences can be realized. The principle of realizing the coupler is as follows. As shown in Figure 3(a), when port 1 is the input port, the TM_{11a} mode is excited in resonator 1. Then, the energy is transmitted to the resonator 2 through microstrip lines connecting the two resonators. Finally, the in-phase output is realized at port 2 and port 3. Similarly, as shown in Figure 3(b), when port 4 is the input port, the TM_{11b} mode is excited in resonator 1. Then, the energy is transmitted to the resonator 2 through microstrip lines connecting the two resonators. Finally, the out-of-phase output is realized at port 2 and port 3. Due to the use of the degenerate mode, good port isolation is realized. In addition, the coupling strength between the two patch resonators can be controlled by changing the width of the microstrip line. So, the bandwidth of the coupler can be flexibly controlled. Figure 4 shows that the bandwidth of the coupler can be flexibly controlled by w_3. In Figures 4(a)–4(d), the bandwidth of the coupler increases when w_3 increases.

In addition, in order to improve the frequency selectivity of the design, two coupling slots are introduced. Two coupling slots which connect the input ports and the output ports are etched on the ground. In this way, the source and load couplings are implemented, resulting in two transmission zeros. Therefore, the coupling between the input ports and the output ports can be controlled through the changing width of the coupling slots. So, the position of transmission zeros can be controlled flexibly. As shown in Figure 5, we can see that the position of the transmission zeros can be flexibly controlled by the width of the coupling slots. In Figures 5(a) and 5(b), we can see that the transmission zeros will move to a higher frequency as k_1 increases. Similarly, in Figures 5(c) and 5(d), the transmission zeros will move to a higher frequency as k_2 increases.

In order to show the working principle more clearly, Figure 6 depicts the coupling topology of the proposed high frequency selectivity filtering coupler. The blue rectangle represents two patch resonators. The solid line indicates the direct coupling, and the dashed line indicates the source and load coupling brought by the coupling slots.

3. Implementation and Results

Through the above analysis, the final dimensions of this filtering coupler are as follows: $w_1 = 1.18$ mm, $w_2 = 0.1$ mm, $w_3 = 1.7$ mm, $w_4 = 0.22$ mm, $w_5 = 0.1$ mm, $l_1 = 44$ mm, $l_2 = 7$ mm, $l_3 = 1.7$ mm, $l_4 = 3$ mm, $l_5 = 4.5$ mm, $l_6 = 0.9$ mm, $l_7 = 8$ mm, $l_8 = 15$ mm, $l_9 = 17$ mm, $l_{10} = 8$ mm, $l_{11} = 17$ mm, $l_{12} = 8$ mm, $l_{13} = 10$ mm, $l_{14} = 14$ mm, $l_{15} = 34$ mm, $l_{16} = 38$ mm, $l_{17} = 18$ mm, $l_{18} = 3$ mm, $l_{19} = 64$ mm, $l_{20} = 63$ mm, $l_{21} = 12$ mm, $l_{22} = 60$ mm, $k_1 = 2$ mm, and $k_2 =$

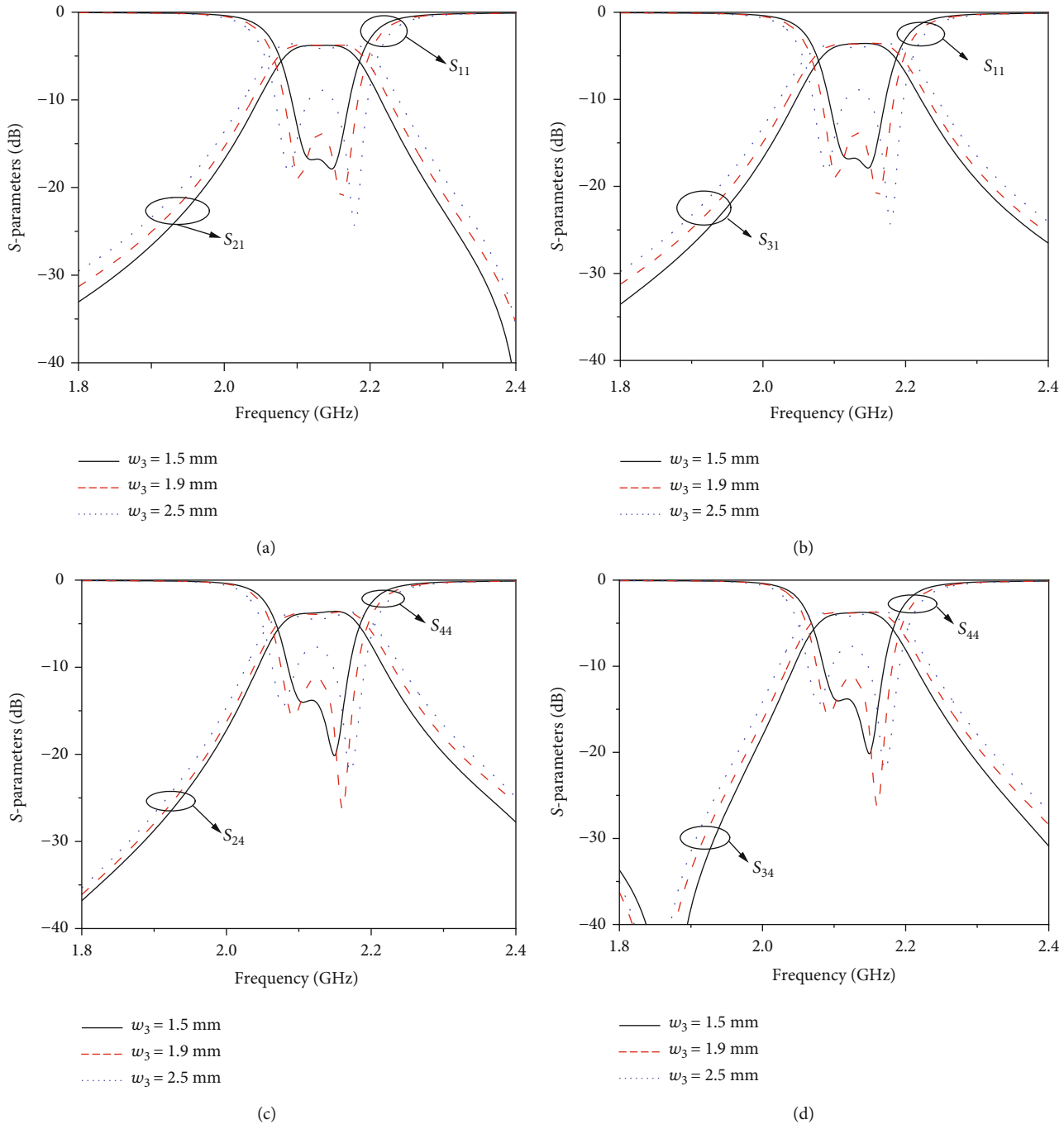

FIGURE 4: (a) Simulated S_{21} and S_{11} under different w_3. (b) Simulated S_{31} and S_{11} under different w_3. (c) Simulated S_{24} and S_{44} under different w_3. (d) Simulated S_{34} and S_{44} under different w_3.

0.4 mm. The substrate used in this design is a Rogers RO4003 with the relative dielectric constant ε_r of 3.55 and thickness of 0.508 mm.

The simulated and measured results are shown in Figure 7. The desired passband is centered at 2.12 GHz. The measured S_{11}, S_{21}, and S_{31} are shown in Figure 7(a). The measured return loss is better than 15 dB, and the measured insertion losses are better than 1.32 dB and 1.43 dB (excluding the 3 dB power division loss). Besides, Figure 7(b) shows the measured S_{44}, S_{24}, and S_{34}, while the return loss is better than 15 dB, and the measured insertion losses are about 1.63 dB and 1.97 dB (excluding the 3 dB power division loss). As shown in Figure 7(c), the measured isolation between port 1 and port 4 within the passband is better than 20 dB, and the return losses of two output ports are better than 15 dB, showing high isolation and good output matching. Figure 7(d) shows that the desire for 0° and 180° phase differences is realized. As shown in Table 1, our work has a wider bandwidth and higher selectivity. The proposed filtering coupler has been manufactured as shown in Figure 8.

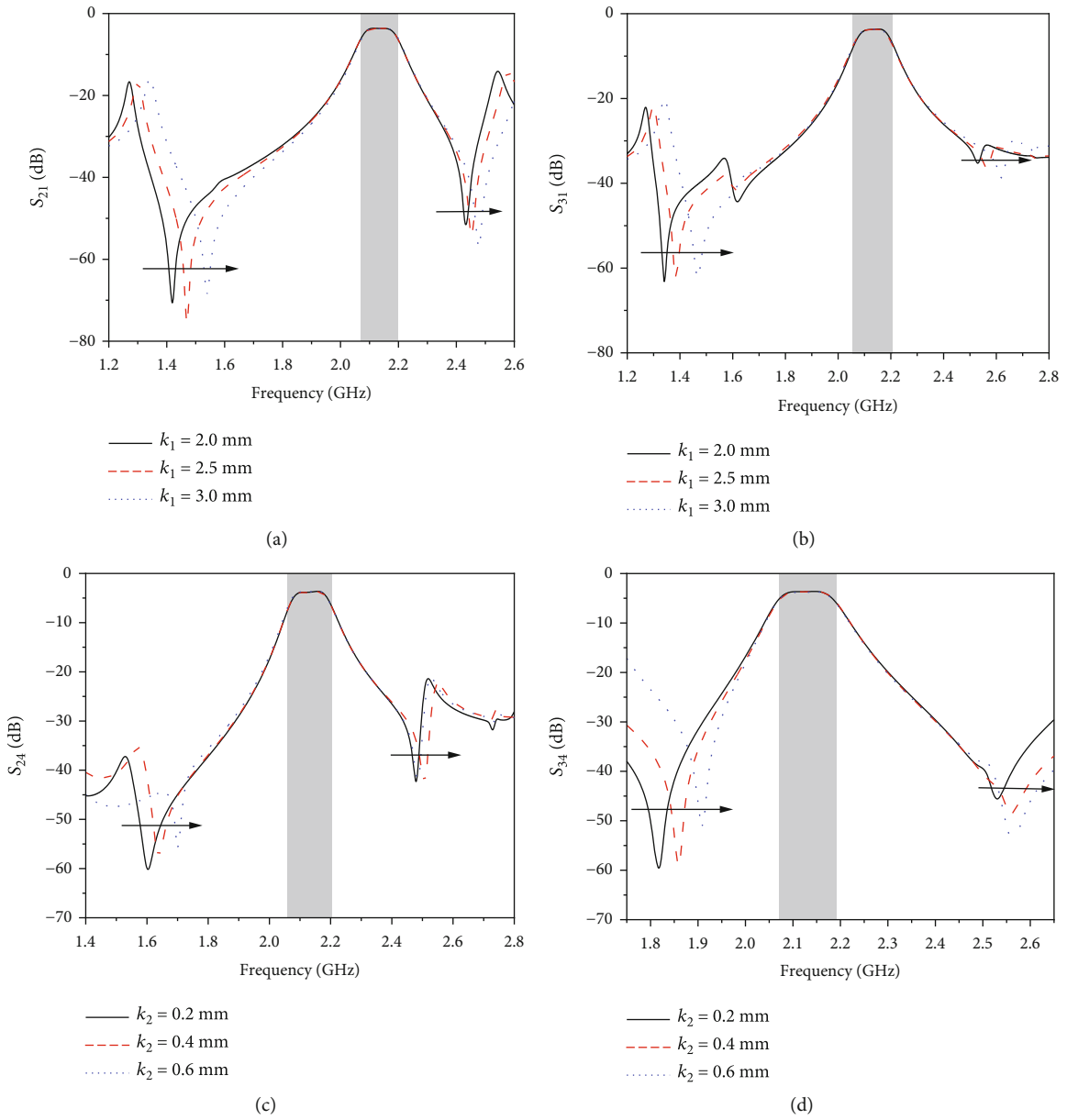

FIGURE 5: (a) Simulated S_{21} under different k_1. (b) Simulated S_{31} under different k_1. (c) Simulated S_{24} under different k_2. (d) Simulated S_{34} under different k_2.

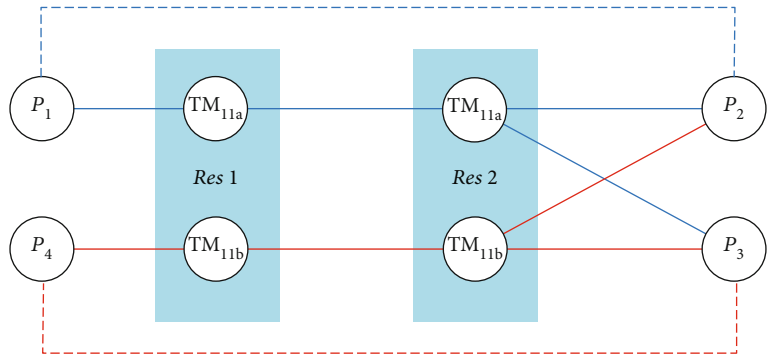

FIGURE 6: The coupling topology of proposed high frequency selectivity filtering coupler.

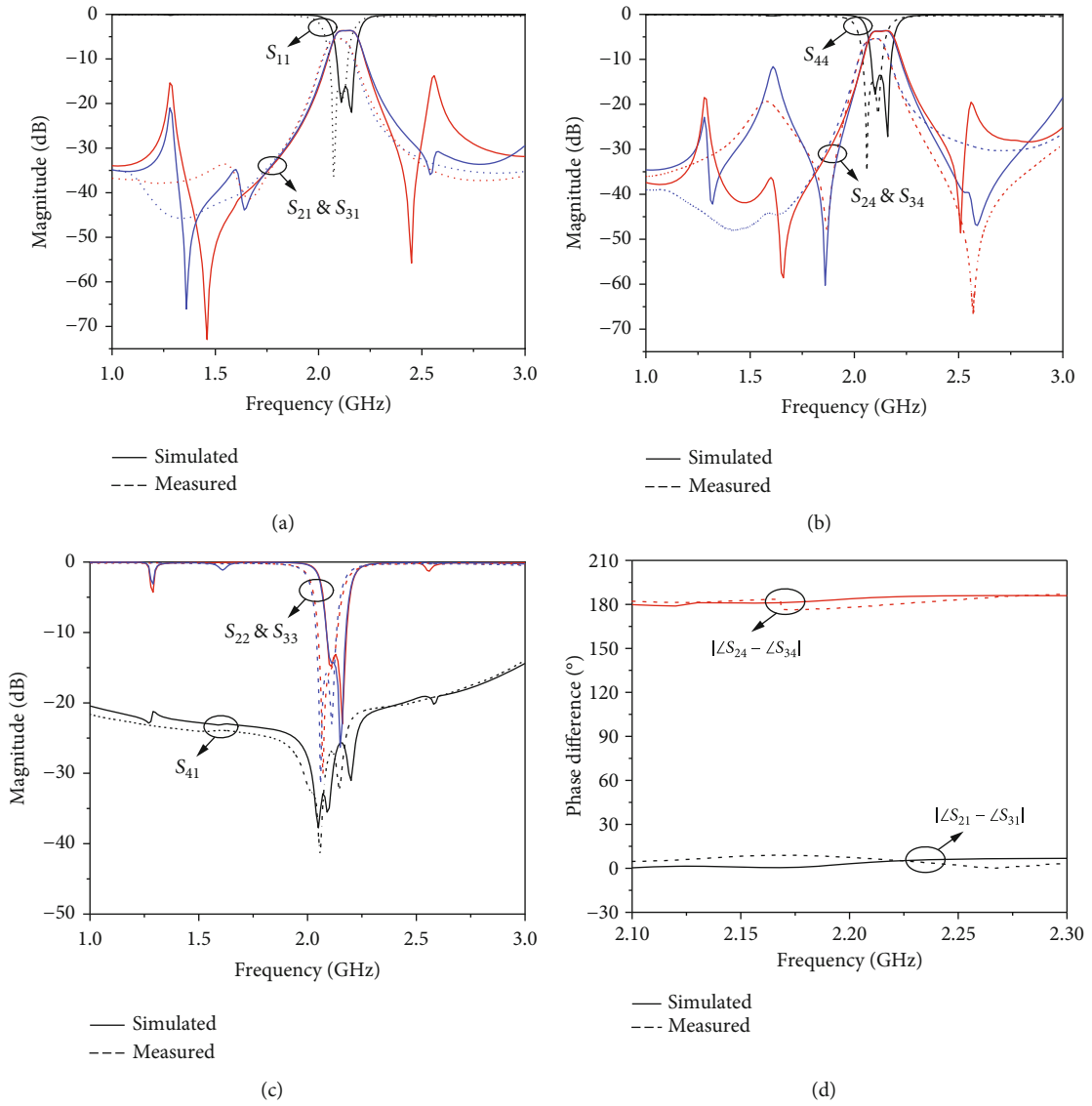

FIGURE 7: Simulated and measured results of filtering coupler. (a) S_{11}, S_{21}, and S_{31} (red and blue lines represent the curves of S_{21} and S_{31}, respectively); (b) S_{44}, S_{24}, and S_{34} (red and blue lines represent the curves of S_{24} and S_{34}, respectively); (c) S_{22}, S_{33}, and S_{41} (red and blue lines represent the curves of S_{22} and S_{33}, respectively); (d) 0° and 180° phase differences between port 2 and port 3.

TABLE 1: Comparisons with other previous works.

Refs.	Size (λ_0*λ_0)	CF (GHz)	3 dB FBW (%)	IL (dB)	Isolation (dB)	Techniques	TZs
[5]	0.095*0.117	0.47	13.3	1.19	-30	Microstrip + LC	2
[7]	1.96*1.96	9	0.77	1.9	-33.2	SIW	0
[10]	0.84*0.84	4.3	16.3	1.3	-28	Patch	2
[11]	1.32*1.32	11.5	0.4	0.25	-25	Waveguide	1
[12]	0.31*0.22	1.5	4	3	-30	Stub-loaded resonators	0
Our work	0.83*0.58	2.12	5.2	1.97	-26	Patch	2

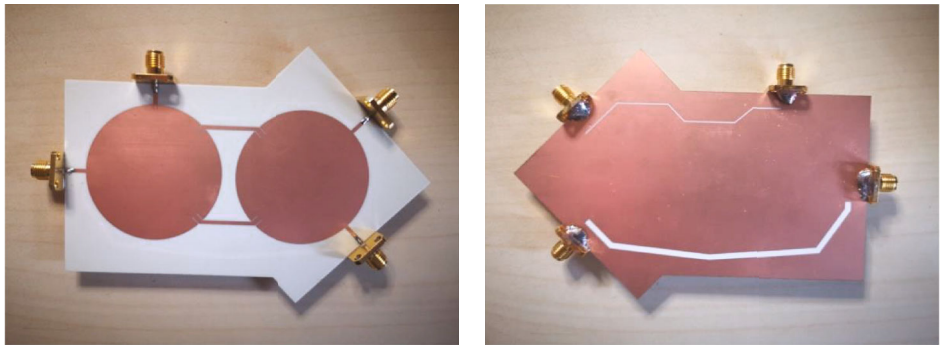

(a) (b)

Figure 8: Photographs of the proposed filtering coupler.

4. Conclusion

This paper presents a new design scheme of a high frequency selectivity planar filtering coupler with both frequency selection and coupler functions. The etched slots are introduced to realize the source-to-load coupling successfully. The design exhibits many advantages in terms of excellent filtering response, high-frequency selectivity, and low profile, etc. These advantages make this filtering coupler have a broad application prospect in LEO satellite communication systems.

Data Availability

The data is already included in the article.

Conflicts of Interest

The authors declare that they have no conflicts of interest.

Acknowledgments

This work was supported in part by the National Natural Science Foundation of China under Grant 62171226 and Postgraduate Research & Practice Innovation Program of Jiangsu Province under Grant SJCX22_0559.

References

[1] Y. Cui, K.-D. Xu, Y.-J. Guo, and Q. Chen, "Half-mode substrate integrated plasmonic waveguide for filter and diplexer designs," *Journal of Physics D: Applied Physics*, vol. 55, no. 12, article 125104, 2022.

[2] H. Uchida, N. Yoneda, Y. Konishi, and S. Makino, "Bandpass directional couplers with electromagnetically-coupled resonators," in *2006 IEEE MTT-S International Microwave Symposium Digest*, pp. 1563–1566, San Francisco, CA, USA, 2006.

[3] K.-X. Wang, X.-F. Liu, Y.-C. Li, Z.-L. Li, and X.-L. Zhao, "LTCC filtering rat-race coupler based on eight-line spatially-symmetrical coupled structure," *IEEE Access*, vol. 6, pp. 262–269, 2018.

[4] W.-H. Wang, T.-M. Shen, T.-Y. Huang, and R.-B. Wu, "Miniaturized rat-race coupler with bandpass response and good stopband rejection," in *2009 IEEE MTT-S International Microwave Symposium Digest*, pp. 709–712, Boston, MA, USA, 2009.

[5] K.-X. Wang, X.-Y. Zhang, S.-Y. Zheng, and Q. Xue, "Compact filtering rat-race hybrid with wide stopband," *IEEE Transactions on Microwave Theory and Techniques*, vol. 63, no. 8, pp. 2550–2560, 2015.

[6] C. K. Lin and S. J. Chung, "A compact filtering 180° hybrid," *IEEE Transactions on Microwave Theory and Techniques*, vol. 59, no. 12, pp. 3030–3036, 2011.

[7] P. Li, H. Chu, and R.-S. Chen, "SIW magic-T with bandpass response," *Electronics Letters*, vol. 51, no. 14, pp. 1078–1080, 2015.

[8] H.-Y. Li, J.-X. Xu, and X.-Y. Zhang, "Substrate integrated waveguide filtering rat-race coupler based on orthogonal degenerate modes," *IEEE Transactions on Microwave Theory and Techniques*, vol. 67, no. 1, pp. 140–150, 2019.

[9] G. Zhang, F. Jiao, S.-C. Liu et al., "Compact single- and dual-band filtering 180° hybrid couplers on circular patch resonator," *IEEE Transactions on Microwave Theory and Techniques*, vol. 68, no. 9, pp. 3675–3685, 2020.

[10] F. Jiao, Q. Zhang, Q.-Y. Zhang, X. Gao, S.-K. Ma, and W.-C. Tang, "Balanced-to-unbalanced filtering magic-T based on circular patch resonator with high selectivity," *Electronics Letters*, vol. 56, no. 23, pp. 1257–1259, 2020.

[11] G. Zhang, Y. Chen, M.-Y. Pan et al., "Design of filtering rat-race coupler based on hemispherical resonator," in *2021 IEEE MTT-S International Microwave Filter Workshop (IMFW)*, pp. 165–168, Perugia, Italy, 2021.

[12] C.-F. Chen, T.-Y. Huang, C.-C. Chen, W.-R. Liu, T.-M. Shen, and R.-B. Wu, "A compact filtering rat-race coupler using dual-mode stub-loaded resonators," in *2012 IEEE/MTT-S International Microwave Symposium Digest*, pp. 1–3, Montreal, QC, Canada, 2012.